Applied Physics Letters ARTICLE scitation.org/journal/apl

Role of deep levels and barrier height lowering in current-flow mechanism in 150 μm thick epitaxial n-type 4H–SiC Schottky barrier radiation detectors

Cite as: Appl. Phys. Lett. **119**, 063502 (2021); doi: 10.1063/5.0064036
Submitted: 19 July 2021 · Accepted: 29 July 2021 ·
Published Online: 10 August 2021

Joshua W. Kleppinger, Sandeep K. Chaudhuri, OmerFaruk Karadavut, and Krishna C. Mandal[a]

AFFILIATIONS

Department of Electrical Engineering, University of South Carolina, Columbia, South Carolina 29208, USA

[a]Author to whom correspondence should be addressed: mandalk@cec.sc.edu

ABSTRACT

Schottky barrier detectors (SBDs) require larger surface areas than conventional electronics to increase the detection efficiency although such SBDs manifest large diode ideality factors due to inhomogeneous areal distribution of surface barrier height (SBH). Inhomogeneous SBH distributions lead to various current flow mechanisms in SBDs, which need to be identified to optimize detector performance. In this Letter, we identify the current flow mechanism in large area Schottky barrier diodes for radiation detection fabricated on 150 μm thick n-4H–SiC epitaxial layers. The analysis of temperature-dependent forward current–voltage (I–V–T) characteristics of SBDs revealed two linear regions in current–voltage curves up to 450 K, one corresponding to the current flow through a low barrier patch, while the other corresponds to that of average barrier distribution. Applying a SBH distribution model to the reverse I–V–T characteristics, an activation energy of 0.76 eV for the current flow over the Schottky barrier was calculated. The activation energy did not directly correspond to any of the defect levels observed from the deep level transient spectroscopy (DLTS). Above 450 K, a Schottky type barrier lowering suggested a current flow through a low barrier patch of $\approx$ 0.8 eV. The absence of any SBH lowering below 450 K indicated that the current corresponded to a neutrally charged trap level at $\approx$ 0.6 eV below the conduction band edge, which was consistent with DLTS measurements revealing the presence of an electron trap level $Z_{1/2}$ at 0.59 eV below the conduction band edge.

At present, semiconductor devices fabricated on the 4H–SiC epitaxial layer are the most suitable choice in harsh environment applications. 4H–SiC radiation detectors have demonstrated their capability at high temperatures and high radiation fields that are normally encountered in high-energy astroparticle physics experiments, nuclear reactor cores, laser-generated plasma environments, and nuclear material storage environments.[1–5] 4H–SiC's success comes from its high average displacement threshold (42 eV for Si and 19 eV for C),[6] which makes it extremely radiation hard, its wide bandgap (3.27 eV at 300 K), and the high degree of crystallinity and low concentration of structural defects in its epilayers, which enables it to achieve excellent charge transport properties, such as a high saturation carrier drift velocity $\sim 10^7$ cm s^{-1} or high breakdown field of 2 MV/cm.[7–9] In general, semiconductor optoelectronic devices require excellent transport properties to demonstrate high energy and temporal resolution.[10,11] Despite 4H–SiC's radiation hardness and high quality of its epitaxial layers, intrinsic and extrinsic defects due to the accumulated radiation dose can degrade the performance of 4H–SiC detectors. These defects act as trapping and recombination centers, which deteriorate the charge transport properties of SiC devices.[12,13] Further discussion on the physics of radiation detection and the role of charge transport can be found in Ref. 14. For the reasons mentioned above, existing 4H–SiC state-of-the-art radiation detectors that provide excellent detector resolution are generally Schottky barrier detectors (SBDs) fabricated on high quality epitaxial layers.[7,8,15–18] A comprehensive review on 4H–SiC as a radiation detection material can be found in a review article by Nava *et al.*[19]

To further the versatility of these detectors, development and fabrication of thick epilayer detectors is on the rise as thin epilayers face difficulty in detecting penetrative radiation, such as x/gamma rays and neutrons.[16,20] However, thick epilayers require much higher bias voltage to fully deplete resulting in substantially more leakage current, which is only amplified under harsh environments with high temperature. High leakage current results in poor signal-to-noise ratio, potentially making the radiation induced detector signals indistinguishable from the detector noise. Thick semi-insulating 4H–SiC has been

considered as an alternative; however, the presence of defects in high concentration inhibits high-resolution radiation detection.[21–23] As such, SBDs require as high surface barrier heights as possible to minimize the leakage current. It should be noted that SBDs for radiation detection are developed with larger contact areas than general electronic devices, such as FETs or MOSFETs, to maximize the detection efficiency of the detectors as the surface (Schottky) contact area also serves as the radiation entrance window. Nonetheless, larger contact areas can introduce spatial inhomogeneities in the barrier height, which can result in a reduced effective barrier height and increased ideality factor at room temperature as well as increased leakage current.[24] In 4H–SiC SBDs, spatial inhomogeneities from low barrier patches are often correlated with dislocations in the surface structure originating from the bulk substrate.[25,26]

Temperature-dependent current–voltage (I–V–T) measurements are a useful tool for delineating non-ideal current components from the ideal. The technique has been applied to find low barrier patches, inhomogeneous barrier distributions, as well as the average barrier height in Schottky diodes with various substrates.[27–29] Under reverse bias, I–V–T characteristic-based techniques have been applied to distinguish among different leakage current mechanisms in Ga_2O_3 Schottky diodes.[30] The present study aims to interpret the temperature dependence of non-ideal currents in a Ni/n-4H–SiC SBD fabricated on 150 μm epitaxial layers, which are sufficiently thick to detect 59.6 keV gamma rays when fully depleted. The leakage current variation was evaluated in terms of non-ideal carrier transport models in conjunction with the results obtained from deep level transient spectroscopy (DLTS) studies. DLTS is a powerful capacitance transient measurement technique, which can be applied to extract deep defect energy levels, capture cross sections, and trap concentrations in semiconductor diodes.[31]

The vertical Schottky barrier detectors were fabricated with circular Ni contacts of area 0.11 cm^2 on 150 μm thick 4H–SiC epitaxial layers. The epitaxial layer was grown on highly conducting 350 μm thick 4H–SiC substrates. Details on the SBD fabrication process of the detector can be found elsewhere.[15] From the capacitance–voltage (C–V) characteristics, the net donor concentration and the average barrier height were calculated to be 2.12×10^{14} cm^{-3} and 2.12 eV at 300 K, respectively. A Keithley 237 source-measure unit was used to record the I–V characteristics of the Schottky diode placed in a temperature-controlled copper stage inside a JANIS VPF800 liquid-nitrogen cryostat controlled by a Lakeshore 325 temperature controller. The C-V and the DLTS measurements were carried out on the same mounting stage with a SULA DDS-12 DLTS system consisting of a double boxcar soft correlator module, a 1 MHz oscillator for capacitance measurements, and a capacitance meter. A detailed description of the DLTS system can be found in our earlier work.[15]

Figure 1 presents the forward bias I–V characteristics of the SBD recorded at temperatures in the range 300–600 K. Based on thermionic emission–diffusion (TED) theory, the dominant current mechanisms in SBDs with moderately doped semiconductor regions are thermionic emission of electrons from the semiconductor side, over the Schottky barrier, to the metal or diffusion of electrons as a result of the electron concentration gradient introduced by the space-charge region. The former is more probable when the majority carrier mobility and the net donor concentration are higher. Under appropriate electric field conditions, both processes can simultaneously play an important

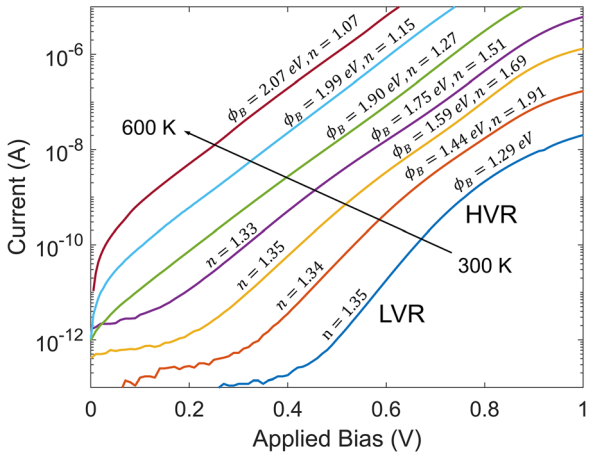

FIG. 1. Forward bias current–voltage characteristics for the Ni/n-4H–SiC Schottky barrier detector fabricated on 150 μ m epitaxial layers from 300 to 600 K measured in steps of 50 K. The ideality factors n and barrier heights Φ_B were acquired by fitting the low voltage region (LVR) and high voltage region (HVR) to Eq. (1) separately. Only a single barrier height is given for each temperature because the calculated barrier height is nearly identical between the two regions. The arrow divides the LVR and HVR.

role in current transport. The way that both processes influence the thermionic emission–diffusion current density J_{TED} in a SDB at a specific temperature T in tandem is described by the following equation:[32,33]

$$J_{TED} = \frac{qN_C v_R}{1 + v_R/v_D} \exp\left(-\frac{\phi_B - \Delta\phi}{kT}\right)\left[\exp\left(\frac{qV}{nkT}\right) - 1\right], \quad (1)$$

where q is the elementary charge of an electron, N_C is the effective density of states of the conduction band, ϕ_B is the Schottky barrier height, $\Delta\phi$ is the Schottky barrier lowering, k is Boltzmann's constant, and n is the ideality factor. v_R (effective Richardson velocity) and v_D (drift velocity) give the relative contribution of thermionic emission vs diffusion. v_R is equal to A^*T^2/qN_C, where A^* is the effective Richardson constant and N_C is the effective density of states of the conduction band, and v_D is approximately equal to μE_m in the depletion region, where μ is the electron mobility. The interfacial electric field is expressed as $E_m = (qN_D/\epsilon) \times d$, where N_D is the net donor concentration, ϵ is the dielectric constant for 4H–SiC, and d is the depletion width. The term outside the bracket in Eq. (1) is called the reverse saturation current I_0. It can be seen from Eq. (1) that J_{TED} is limited by the slower process between thermionic emission and diffusion. For high carrier mobility and highly doped devices, $v_D \approx \mu E_m \gg v_R$, and hence, Eq. (1) converges to the conventional thermionic emission model. Under such circumstances, a semi-logarithmic plot of the current density as a function of the bias voltage would be linear whose slope determines the ideality factor n. However, based on the C–V measurements of the present device, the doping concentration and the interfacial electric field are too low for the above assumption to be valid, and thus, the full TED model must be applied in the analysis. Temperature dependent I–V traces in Fig. 1 clearly show that above 300 K and below 500 K, there are two linear regions in each I–V trace each with its own separate ideality factor. This type of behavior

has been attributed to defects distorting the barrier height distribution effectively creating two types of barrier height distributions.[34,35] This has been observed in the I–V–T results of other 4H–SiC Schottky diodes and is more likely to occur in diodes with larger contact diameters.[34,36,37] The ideality factor for the low voltage region (LVR) was calculated to be 1.34 ± 0.01 for all the temperatures up to 450 K, while that for the high voltage region (HVR) was seen to vary with temperature. The LVR disappears at high temperatures making the HVR and high temperature regions equivalent. In the HVR, the ideality factor was found to be as high as 1.90 ± 0.02 at 350 K and seen to decrease with rising temperature. Interestingly, at even higher temperatures ($\geq$500 K), the ideality factor decreased from 1.27 at 500 K to 1.07 at 600 K. Barrier heights in the HVR increase with the increasing temperature from 1.29 ± 0.01 eV at 300 K to 2.07 eV at 600 K.

Let us focus on the variation of ideality factor in the HVR. The relationship between the barrier height and ideality factor at all the measurement temperatures, including the high temperature region, is seen to be linear as shown in Fig. 2(a). This behavior indicates an inhomogeneous barrier distribution about the average barrier height wherein the net current is the sum of all the currents passing through each individual patches (I_i) with their own area (A_i) and surface barrier height (ϕ_i).[27,35] As such, the measured barrier height is an effective value based on the amount of current passing through each patch and is reduced compared to the average barrier height usually obtained from capacitance–voltage measurements as current tends to flow through the lower barrier patches. The effective current is defined by the Boltzmann distribution of the region's barrier height and is given as follows:[35]

$$I = \sum_i I_i = A^* T^2 \left[\exp\left(\frac{qV}{kT}\right) - 1\right] \sum_i \exp\left(-\frac{\phi_i}{kT}\right) A_i. \quad (2)$$

The above equation suggests that at relatively low temperatures the low barrier patch (high ϕ_i) terms in the summation are the significant contributors to the effective current. However, at high temperatures, the pre-factor on the right-hand side fades away and the high barrier patch terms are the ones, which become significant contributors, causing the effective barrier height to resemble the average barrier height. In the present detector, the ideality factor swings from $\approx$2 to $\approx$1 in the temperature range of 350–600 K, which implies that the spatial variation of the Schottky barrier is substantial. This is attributed to the combination of the larger contact area and high average barrier height of the SBD. Since the relationship between the ideality factor and effective barrier height of the HVR is linear, the average barrier height can be estimated from the y-intercept at $n = 1$ of the linear fit of the plot in Fig. 2(a). For the present detector, this is calculated to be 2.11 ± 0.02 eV, which is nearly the same as what was acquired from the C–V and is approximately the theoretical limit for Ni/n-4H–SiC SBDs.

The LVR gives additional insight on the surface structure and current flow. A plot of $I_0/(N_c.v_{eff})$ vs $1/kT$ as displayed in Fig. 2(b) shows a linear variation on a log scale. Based on Tung's model,[35] this indicates the presence of a single dominant low barrier patch with a barrier height (φ_p) and effective area (A_p) of 0.93 ± 0.01 eV and 2.60×10^{-10} cm^2, respectively. The potential impact of this low barrier patch on the leakage current relative to rest of the surface barrier can be evaluated by taking the ratio of the reverse saturation current of the low barrier patch I_{p0} (defined as the LVR's I_0) to the reverse saturation current I_s through the rest of the Schottky barrier (defined by the HVR's I_0),

$$(I_{r0}/I_s) = \left(\frac{A_p}{A}\right) \exp\left(-\frac{\phi_p - \phi_B(T)}{kT}\right), \quad (3)$$

where A ($= 0.11$ cm^2) and $\phi_B(T)$ are the area of the top Schottky contact and effective barrier height of the HVR at each temperature, respectively. If the ratio is less than one, then more current passes through the effective Schottky barrier, whereas if it is greater, more current will pass through the low barrier patch instead. At room temperature, this ratio is calculated to be on the order of 10^{-3} for the present detector, implying that the leakage current passing through the low barrier patch is comparatively negligible. However, because the effective barrier height increases with temperature, the ratio increases to approximately 0.5 at 400 K and further to a maximum of $\approx$14 at

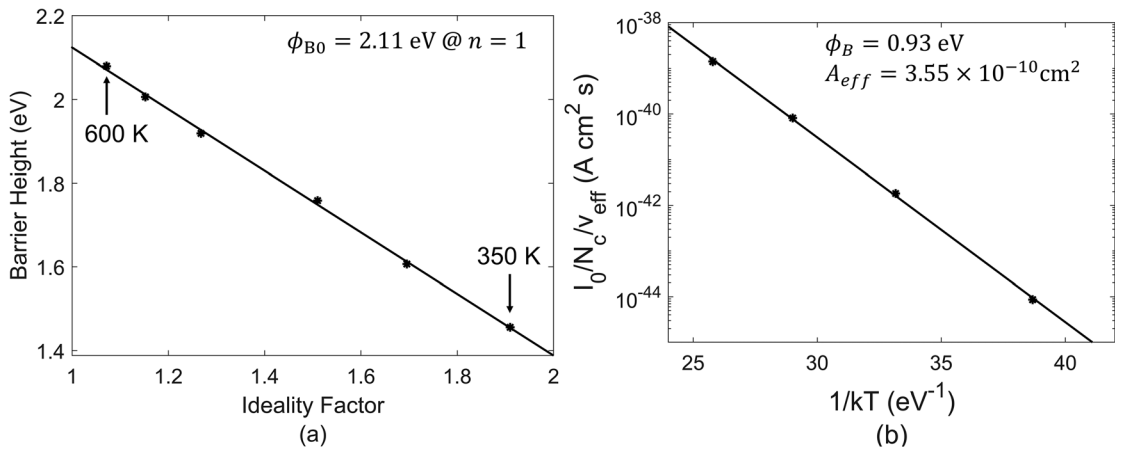

FIG. 2. Barrier height plotted against its corresponding ideality factor in the HVR (a) and the Arrhenius plot of the saturation current I_0 divided by $N_c v_{eff}$ of the LVR (b). The high temperature region ($\geq$ 500 K) is included as part of the HVR for (a), and the solid line is the linear fit used to acquire the average barrier height Φ_{B0}. The effective carrier velocity v_{eff} is defined as the $v_R/(v_R + v_D)$ term in Eq. (1).

500 K, and therefore, more leakage current will pass through the patch instead.

Figure 3(a) shows the reverse bias leakage current of the detector as a function of the electric field at the metal-semiconductor interface, which is seen to be linear in the field range 20–80 kV/cm (4–80 V) for temperatures ranging from 400 to 600 K. The leakage currents at 300 and 350 K are nonlinear, and the current growth from 300 to 400 K has a very weak temperature dependence. In the temperature range of 400–600 K, the temperature dependence of the slope of I vs E_m plots, as shown in Fig. 3(b), is observed to be exponential with an overall activation energy of 0.76 ± 0.02 eV. If the leakage current were solely due to the current passing through the low barrier region, one would expect the activation energy to match the barrier height of the LVR (0.93 eV). Another possible explanation for the observed linearity in the leakage current vs electric field plot is that deep level defects are assisting in the transport of electrons through the space charge region. Through a process of being repeatedly trapped and de-trapped, electrons will slowly drift in the direction of the electric field and, thus, the current will vary linearly with the electric field. This type of current transport is generally referred to as the Poole-Frenkel (PF) emission and is mathematically described as below:[38,39]

$$J_{PF} = q\mu n_0 E_m \exp\left(-\frac{\phi_t - \Delta\phi}{kT}\right), \tag{4}$$

where μn_0 is the mobility-carrier density product, ϕ_t is the trap barrier height measured from the conduction band edge (CBE), and $\Delta\phi$ is the barrier lowering. The above-determined activation energies of 0.6–0.7 eV usually indicate the presence of $Z_{1/2}$ traps generally linked to carbon vacancy related complexes.[40–42] However, 0.76 eV is relatively high for $Z_{1/2}$. This value is closer to the S_2 trap corresponding to silicon vacancies, but this level is unlikely to appear in as-grown epilayers due to its extremely high formation energy.[43,44]

To identify whether any other defect is responsible for a possible defect assisted electron transport, DLTS studies were carried out in the detector under investigation. Capacitance-mode DLTS spectra were acquired using a steady-state bias of –5 V and a 0 V filling pulse of the 1 μs width. Spectra were acquired using correlator delays from 0.5 to 100 ms over the temperature range of 80–750 K in steps of 1 K, which can resolve a wide range of defects with activation energies ranging from 0.15 to 1.8 eV. The DLTS scans simultaneously acquired for four correlators are shown in Fig. 4(a), showing 4 peaks marked as Ti(c), EH_1, $Z_{1/2}$, and $EH_{6/7}$. The corresponding Arrhenius plots for all the peaks are shown in Fig. 4(b). The first peak corresponds to 0.19 ± 0.01 eV below the conduction band is related to titanium impurities at the cubic silicon site.[45] The central peak is identified as $Z_{1/2}$ at 0.59 ± 0.01 eV below the CBE, and its left shoulder at 0.48 ± 0.01 eV is likely the EH_1 trap center reported by Castaldini *et al.*[46] The fourth peak labeled $EH_{6/7}$ in Fig. 4(a) was calculated to be located at 1.35 ± 0.03 eV below the CBE.[47] This is relatively low for $EH_{6/7}$. However, the corresponding trap concentration is practically identical to that of $Z_{1/2}$ ($\approx 2\times10^{11}$ cm^{-3}) and no other defects with higher energy were observed in this detector. Since both $Z_{1/2}$ and $EH_{6/7}$ are usually correlated and attributed to two different charge states of the carbon vacancy, the most reasonable assignment of this level is $EH_{6/7}$.[44,46–49] It is clear from the above results that 0.76 eV does not directly correspond to any deep level displayed in the DLTS spectrum.

The nature of the current transport can be further interpreted from its barrier lowering, which is proportional to the square root of the electric field and expressed by[32,38,39]

$$\Delta\phi = \frac{1}{m}\sqrt{\frac{qE_m}{\pi\epsilon}}. \tag{5}$$

In the above equation, m is the barrier lowering parameter and ϵ is the electrical permittivity of the semiconductor. The value of $m \approx 2$ implies Schottky lowering, whereas $m \approx 1$ indicates Poole–Frenkel lowering. Thus, the barrier lowering can be evaluated from the $\ln(J/E_m)$ vs $E_m^{1/2}$ plot, which is presented in Fig. 5. From the linear fit to the plot, m is found to be greater than 4 up to 450 K. For comparison, in the electric field range considered, the barrier lowering is expected to be ≈ 0.04–0.05 eV for $m = 1$. In terms of trap-assisted conduction, this indicates that the defect lacks a Coulombic potential and, therefore, must be neutrally charged when empty.[48–51] At 500 and 550 K, the barrier lowering parameter is approximately 2, indicating Schottky lowering. At 600 K, it is 1.48 indicating a combination of

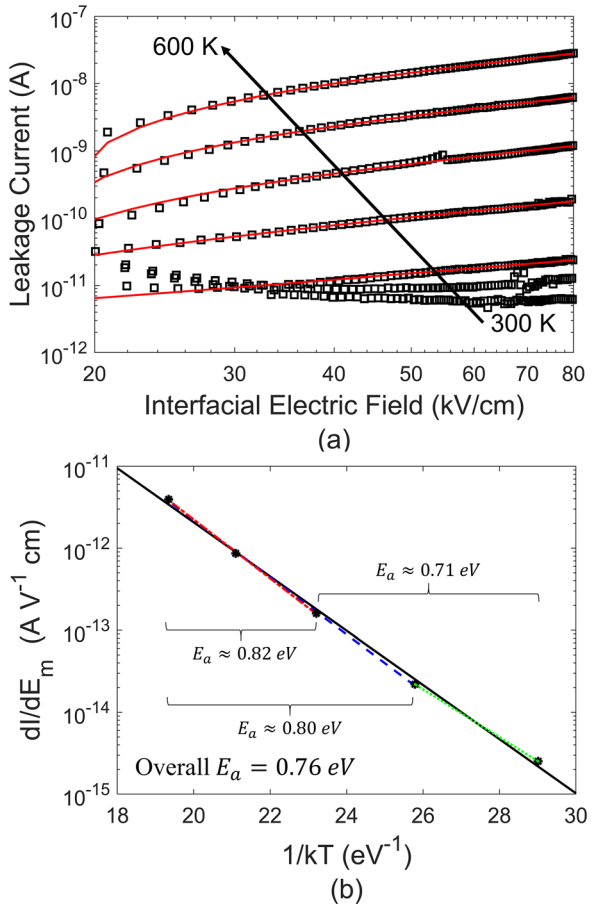

FIG. 3. Reverse bias leakage current as a function of the electric field at metal–semiconductor interface on a log–log scale (a) and the Arrhenius plot of the slopes of each *I–V* trace from 20 to 80 kV/cm (b). The solid lines in plots are the linear fit to the data points, whereas the dashed and dotted lines in (b) correspond to linear fits over a reduced temperature range marked by the braces.

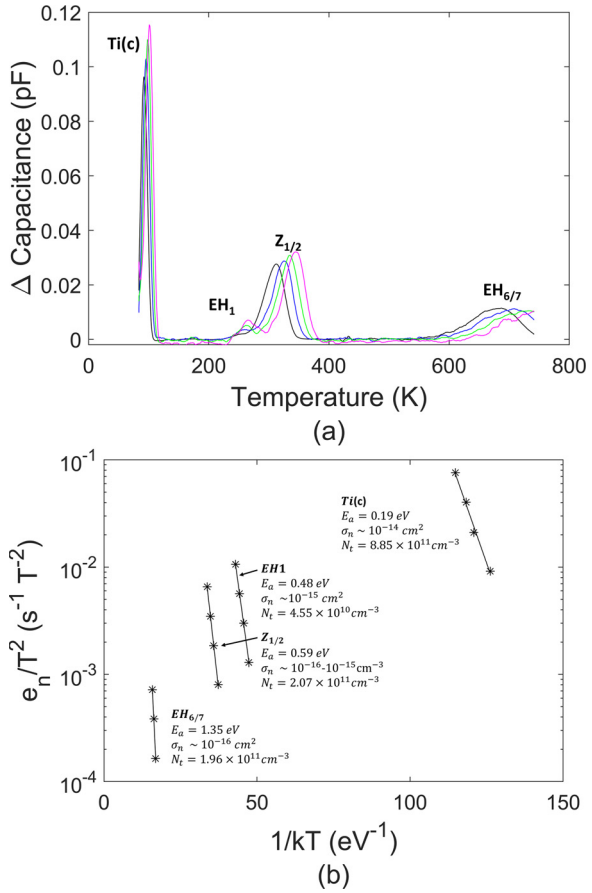

FIG. 4. DLTS spectra of the detector acquired from 80 to 750 K for four different rate windows corresponding to initial delays 0.5, 1, 2, and 5 ms. (a) and the Arrhenius plot of the emission rates corresponding to the peaks in the spectra (b). The rate window is defined as (4.3 × initial delay) in ms.

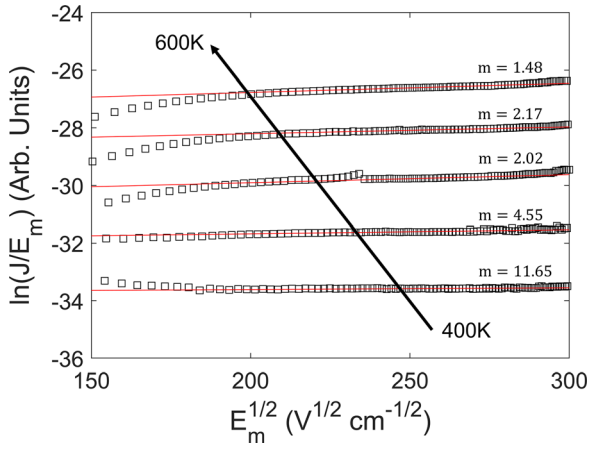

FIG. 5. Natural logarithm of the reverse bias leakage current normalized to the interfacial electric field plotted against the square root of the interfacial electric field. The parameter *m* is the barrier lowering parameter defined in Eq. (5).

different types of lowering. Overall, this suggests that the linear increase in the reverse leakage current with the increasing electric field below and above 450 K is the results of two separate, possibly overlapping, phenomena. Indeed, if the range of the Arrhenius plot in Fig. 3(b) is adjusted to exclude 400 K, the activation energy increases to 0.80 ± 0.01 eV—even more so if both 400 K and 450 K are excluded from the fitting. Conversely, the activation energy decreases to 0.71 eV if the data points corresponding to 550 and 600 K are excluded from the fitting. The activation energy of 0.76 eV is likely the average of a low barrier patch—possibly the same as extracted from forward bias characteristics—of barrier height > 0.8 eV and an additional current source with activation energy < 0.7 eV prevalent at ≤ 450 K. Since linearity is observed up to 80 kV/cm, the source of the low barrier patch could be a threading dislocation with reduced mobility compared to the bulk mobility. Given the probable activation energy and the lack of barrier lowering, the source of the leakage current from 400 to 450 K could be $Z_{1/2}$ assisted, which corresponds to the neutral carbon vacancy when empty.[50] We conclude that linear behavior with the electric field and temperature dependence of the leakage current is the result of a combination of leakage current through a low barrier patch and conduction from $Z_{1/2}$ found in the DLTS spectrum. The two effects were differentiated from the temperature dependence of the barrier lowering.[49,50]

This work was supported by the DOE Office of Nuclear Energy's Nuclear Energy University Program (NEUP), Grant Nos. DE-AC07-051D14517 and DE-NE0008662. The work was also supported in part by the Advanced Support Program for Innovative Research Excellence-I (ASPIRE-I), Grant No. 15530-E404 and Support to Promote Advancement of Research and Creativity (SPARC), Grant No. 15530-E422 of the University of South Carolina (U*of*SC), Columbia, USA.

DATA AVAILABILITY

The data that support the findings of this study are available from the corresponding author upon reasonable request.

REFERENCES

[1]N. R. Taylor, Y. Yu, M. Ji, T. Aytug, S. Mahurin, R. Mayes, S. Cetinar, M. Paras Paranthanam, D. Ezell, L. R. Cao, and P. C. Joshi, Appl. Phys. Lett. **116**, 252108 (2020).
[2]V. V. Kozlovski, A. A. Lebedev, M. E. Levinshtein, S. L. Rumyanstev, and J. W. Palmour, J. Appl. Phys. **123**, 024502 (2018).
[3]G. Bertuccio, D. Puglisi, L. Torrisi, and C. Lanzieri, Appl. Surf. Sci. **272**, 128 (2013).
[4]K. C. Mandal, J. W. Kleppinger, and S. K. Chaudhuri, Micromachines **11**, 254 (2020).
[5]M. C. Miller and D. A. Vega, Nucl. Eng. Technol. **45**, 803 (2013).
[6]G. Lucas and L. Pizzagalli, Nucl. Instrum. Methods Phys. Res., Sect. B **229**, 359 (2005).
[7]B. Zat'ko, F. Dubecký, A. Šagátová, K. Sedlačová, and L. Ryć, J. Instrum. **10**, C04009 (2015).
[8]S. K. Chaudhuri, K. J. Zavalla, and K. C. Mandal, Nucl. Instrum. Methods Phys. Res., Sect. A **728**, 97 (2013).
[9]S. Nakamura, H. Kumagai, T. Kimoto, and H. Matsunami, Appl. Phys. Lett. **80**, 3355 (2002).
[10]S. O. Kasap, M. Z. Kabir, K. O. Ramaswami, R. E. Johanson, and R. J. Curry, J. Appl. Phys. **128**, 124501 (2020).
[11]M. Z. Kabir, E. V. Emelianova, V. I. Arkhipov, M. Yunus, S. O. Kasap, and G. Adriaenssens, J. Appl. Phys. **99**, 124501 (2006).

[12]Y. Fang, X. Wu, J. Yang, G. Chen, Y. Chen, Q. Wu, and Y. Song, Appl. Phys. Lett. **112**, 201904 (2018).
[13]C.-Y. Cheng and D. Vasileska, J. Appl. Phys. **127**, 155702 (2020).
[14]G. F. Knoll, *Radiation Detection and Measurement* (John Wiley & Sons, Inc. New York, 2011).
[15]S. K. Chaudhuri, J. W. Kleppinger, and K. C. Mandal, J. Appl. Phys. **128**, 114501 (2020).
[16]D. Puglisi and G. Bertuccio, Micromachines **10**, 835 (2019).
[17]C. S. Bodie, G. Lioliou, and A. M. Barnett, Nucl. Instrum. Methods Phys. Res., Sect. A. **985**, 164663 (2021).
[18]Y. M. Abubakar, A. Lohstroh, and P. Sellin, IEEE Trans. Nucl. Sci. **62**, 2360 (2015).
[19]F. Nava, G. Bertuccio, A. Cavallini, and E. Vittone, Meas. Sci. Technol. **19**, 102001 (2008).
[20]J. Wu, Y. Jiang, M. Li, L. Zeng, J. Li, H. Gao, D. Zou, Z. Bai, C. Ye, W. Liang, S. Dai, Y. Lu, R. Rong, J. Du, and X. Fan, Rev. Sci. Instrum. **88**, 083301 (2017).
[21]W. Cunningham, A. Gouldwell, G. Lamb, J. Scott, K. Mathieson, P. Roy, R. Bates, P. Thornton, K. M. Smith, R. Cusco, M. Glaser, and M. Rahman, Nucl. Instrum. Methods Sci. Res., Sect. A **487**, 33 (2002).
[22]G. Bertuccio, D. Puglisi, A. Pullia, and C. Lanzieri, IEEE Trans. Nucl. Sci. **60**, 1436 (2013).
[23]P. G. Muzykov, R. M. Krishna, and K. C. Mandal, J. Appl. Phys. **111**, 014910 (2012).
[24]E. Dobročka, Appl. Phys. Lett. **65**, 575 (1994).
[25]S. I. Maximenko, J. A. Freitas, R. L. Myers-Ward, K. K. Lew, B. L. VanMil, C. R. Eddy, D. K. Gaskill, P. G. Muzykov, and T. S. Sudarshan, J. Appl. Phys. **108**, 013708 (2010).
[26]Y. Wang, G. N. Ali, M. K. Mikhov, V. Vaidyanathan, B. J. Skromme, B. Raghothamachar, and M. Dudley, J. Appl. Phys. **97**, 013540 (2005).
[27]R. F. Schmitsdorf, T. U. Kampen, and W. Mönch, J. Vac. Sci. Technol. B **15**, 1221 (1997).
[28]B. J. Skromme, E. Luckowski, K. Moore, M. Bhatnagar, C. E. Weitzel, T. Gehoski, and D. Ganser, J. Electron. Mater. **29**, 376 (2000).
[29]Q. Feng, Z. Feng, Z. Hu, X. Xing, G. Yan, J. Zhang, Y. Xu, X. Lian, and Y. Hao, Appl. Phys. Lett. **112**, 072103 (2018).
[30]W. Li, K. Nomoto, D. Jena, and H. G. Xing, Appl. Phys. Lett. **117**, 222104 (2020).
[31]D. V. Lang, J. Appl. Phys. **45**, 3023 (1974).
[32]E. H. Rhoderick, IEEE Proc. I - Solid State Electron Dev. **129**, 1 (1982).
[33]S. M. Sze and K. K. Ng, *Physics of Semiconductor Devices* (John Wiley & Sons, New York, 2007).
[34]F. Triendl, G. Pfusterschmied, G. Pobegen, J. P. Konrath, and U. Schmid, Semicond. Sci. Technol. **35**, 115011 (2020).
[35]R. T. Tung, Phys. Rev. B **45**, 13509 (1992).
[36]D. Defives, O. Noblanc, C. Dua, C. Brylinski, M. Barthula, V. Aubry-Fortuna, and F. Meyer, IEEE Trans. Electron Devices **46**, 449 (1999).
[37]G. Brezeanu, G. Pristavu, F. Draghici, M. Badila, and R. Pascu, J. Appl. Phys. **122**, 084501 (2017).
[38]H. Schroeder, J. Appl. Phys. **117**, 215103 (2015).
[39]P. Samanta and K. C. Mandal, J. Appl. Phys. **121**, 034501 (2017).
[40]J. Zhang, L. Storasta, J. P. Bergman, N. T. Son, and E. Janzén, J. Appl. Phys. **93**, 4708 (2003).
[41]K. Danno, T. Kimoto, and H. Matsunami, Appl. Phys. Lett. **86**, 122104 (2005).
[42]M. A. Mannan, S. K. Chaudhuri, K. V. Nguyen, and K. C. Mandal, J. Appl. Phys. **115**, 224504 (2014).
[43]T. Hornos, A. Gali, and B. G. Svensson, Mater. Sci. Forum **679–680**, 261 (2011).
[44]J. W. Kleppinger, S. K. Chaudhuri, O. Karadavut, and K. C. Mandal, J. Appl. Phys. **129**, 244501 (2021).
[45]T. Dalibor, G. Pensl, N. Nordell, and A. Schöner, Phys. Rev. B **55**, 13618 (1997).
[46]A. Castaldini, A. Cavallini, L. Rigutti, F. Nava, S. Ferrero, and F. Giorgis, J. Appl. Phys. **98**, 053706 (2005).
[47]G. Alfieri and T. Kimoto, Appl. Phys. Lett. **102**, 152108 (2013).
[48]K. Kawahara, X. Thang Trinh, N. Tien Son, E. Janzén, J. Suda, and T. Kimoto, J. Appl. Phys. **115**, 143705 (2014).
[49]P. G. Muzykov, R. M. Krishna, and K. C. Mandal, Appl. Phys. Lett. **100**, 032101 (2012).
[50]J. W. Kleppinger, S. K. Chaudhuri, and K. C. Mandal, Proc. SPIE **11494**, 114940 (2020).
[51]L. Gordon, A. Janotti, and C. G. Van de Walle, Phys. Rev. B **92**, 045208 (2015).